

A new model to simulate the elastic properties of mineralized collagen fibril

Fang Yuan · Stuart R. Stock · Dean R. Haeffner ·
Jonathan D. Almer · David C. Dunand ·
L. Catherine Brinson

Received: 6 December 2009 / Accepted: 3 May 2010 / Published online: 3 June 2010
© Springer-Verlag 2010

Abstract Bone, because of its hierarchical composite structure, exhibits an excellent combination of stiffness and toughness, which is due substantially to the structural order and deformation at the smaller length scales. Here, we focus on the mineralized collagen fibril, consisting of hydroxyapatite plates with nanometric dimensions aligned within a protein matrix, and emphasize the relationship between the structure and elastic properties of a mineralized collagen fibril. We create two- and three-dimensional representative volume elements to represent the structure of the fibril and evaluate the importance of the parameters defining its structure and properties of the constituent mineral and collagen phase. Elastic stiffnesses are calculated by the finite element method and compared with experimental data obtained by synchrotron X-ray diffraction. The computational results match the experimental data well, and provide insight into the role of the phases and morphology on the elastic deformation characteristics. Also, the effects of water, imperfections in the mineral phase and mineral content outside the mineralized collagen fibril upon its elastic properties are discussed.

Keywords Bone · Collagen fibril · Modeling · Finite element analysis · Structure-property relationship

1 Introduction

Bones are important natural materials. One fundamental function of bone is mechanical—to provide a robust, lightweight frame to support the body and movement. To fulfill this essential function, bone has evolved a complex hierarchical structure with exceptional mechanical characteristics: it combines the high stiffness of the mineral phase (mainly hydroxyapatite) and the high toughness of the organic phase (mainly collagen) (seen in Fig. 1) (Ashby 1993; Fratzl and Weinkamer 2007; Oyen 2008). Bone and related biological materials (i.e., dentin, enamel and antlers) are optimized composites whose properties lie on or near the upper bound of the possible composite properties given by the constituents (Fig. 1). This remarkable characteristic is the consequence of the complex hierarchical structure of bone.

Therefore, the varied structural architecture of bone at different length scales is intensively studied, and there are several excellent reviews describing the hierarchical structure of bone (Fratzl and Weinkamer 2007; Meyers et al. 2008; Rho et al. 1998; Weiner and Wagner 1998). From macroscopic to microscopic level, the structure of bone can be divided into five levels: (1) macrostructure level: cancellous and cortical bone; (2) microstructure level (from 10 to 500 microns): osteons, Haversian systems and trabeculae; (3) sub-microstructure level (from 1 to 10 microns): lamellae and mineralized collagen fibers; (4) nanostructure level (from a few hundred nanometers to 1 micron): mineralized collagen fibrils; and (5) the sub-nanostructure level (below a few hundred nanometers): molecular and atomic structure of major components (Rho et al. 1998; Weiner and Wagner 1998).

F. Yuan · D. C. Dunand · L. C. Brinson
Department of Materials Science and Engineering, Northwestern
University, 2220 Campus Drive, Evanston, IL 60208, USA

S. R. Stock
Department of Molecular Pharmacology and Biological Chemistry,
Northwestern University, 303 E. Chicago, Chicago, IL 60611, USA

D. R. Haeffner · J. D. Almer
Advanced Photon Source, Argonne National Laboratory,
9700 S. Cass Avenue, Argonne, IL 60439, USA

L. C. Brinson (✉)
Department of Mechanical Engineering, Northwestern University,
2145 Sheridan Road, Evanston, IL 60208, USA
e-mail: cbrinson@northwestern.edu

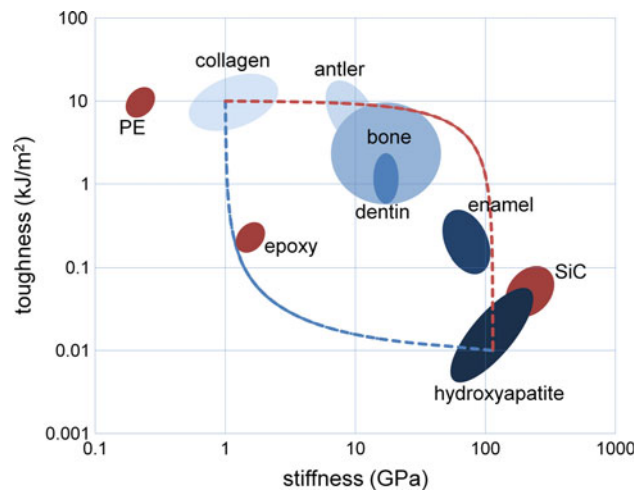


Fig. 1 Plot of toughness vs. stiffness for bone and related biological materials which are mainly composed of collagen and hydroxyapatite. The dotted lines are the upper and lower bounds of the possible composites using these two phases. All the biological materials in the picture lie on or near the upper bound (calculated by using equations given by Ashby 1993). Three reference materials (polyethylene, epoxy and silicon carbide) are also shown (Fratzl and Weinkamer 2007)

At the higher levels, bone is adapted diversely with different structures and functions. However, when bone is investigated at the lower level, the structure of mineralized collagen fibril is similar; therefore, mineralized collagen fibrils are considered as the basic building blocks of bone (Weiner and Wagner 1998).

The mineralized collagen fibril can be considered as a nanocrystal-reinforced composite. The nanocrystals in the mineralized collagen fibril are calcium-based mineral, a defective form of hydroxyapatite (Dorozhkin and Epple 2002). The most important component of the matrix in the composite is type-I collagen, which is composed of triple-helical polypeptide chain molecules (Orgel et al. 2006). In the matrix, in addition to type-I collagen, there are hundreds of non-collagenous proteins (Delmas et al. 1984). However, because of their small volume fraction (altogether <10% of total organic components) and lack of evidence of direct relationship with mechanical properties, these secondary proteins are typically ignored in deformation studies (Currey 2003). Another important component of bone is water, which influences the properties of bone significantly: wet bone (natural state) and dry bone have very different mechanical responses (Nyman et al. 2006).

The mineralized collagen fibril has a cylindrical shape with a diameter of about 200 nm (Parry and Craig 1984). It is difficult to identify the exact length of mineralized collagen fibrils because they tend to merge with neighboring ones (Birk et al. 1991), but the measurement of rat-tail tendons (unmineralized collagen fibril) indicated the length is always longer than 10 μm (Craig et al. 1989). Within the mineralized collagen fibril, it is well established that the mineral

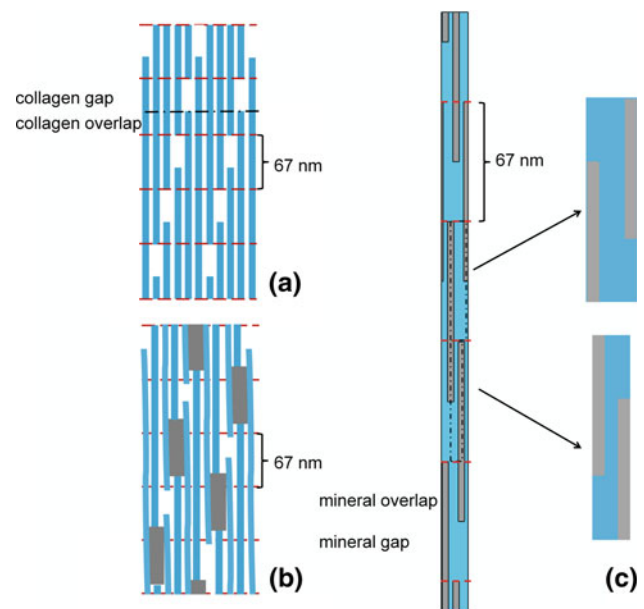


Fig. 2 2-D sketch of the staggered pattern in mineralized collagen fibril. **a** The unmineralized collagen matrix. The blue regions represent collagen chain molecules. A periodicity of 67 nm along the axial direction is shown. Within one period, there is a gap region and an overlap region of the collagen molecules (the white regions represent the space between the collagen chain molecules, not drawn to scale). **b** The mineralized collagen fibril. The mineral phase (gray region) nucleates and grows in the gap regions of collagen matrix at first and penetrates into overlap regions in the later stages. The growing mineral phase occupies the space of collagen phase and deforms the shape of collagen chain molecules. **c** The mineralized collagen fibril drawn as two-phase composite to scale (the gray region is mineral phase and the blue region is collagen phase). The mineral plates in the mineralized collagen fibril show a staggered pattern along the axial direction with the period of 67 nm with alternating gap and overlap regions. Two different RVEs are shown on the right

phase is plate like in shape. The size of the mineral plates varies among different kinds of bones, different animals and even different measurement techniques, e.g., transmission electron microscopy (TEM) and small-angle X-ray scattering (SAXS) (Posner 1969). A wide range of mineral plate dimensions has been reported in the literature: 15–150 nm in length, 10–80 nm in width and 2–7 nm in thickness, while the distance between the neighboring plates is on same the order as the thickness (Rubin et al. 2003).

Experiments have shown that the mineral plates in the collagen matrix are in a staggered pattern along the axial direction of mineralized collagen fibril (Hassenkam et al. 2004). The staggered pattern was also proposed by Jäger and Fratzl (2000), which was deduced from the mechanical properties of mineralized collagen fibril, as shown in Fig. 2. In Fig. 2a, the collagen matrix shows a periodicity in the axial direction, which is consistent with the peaks in SAXS patterns (Hulmes 2002). The length of collagen chain molecule is about 300 nm (Orgel et al. 2001), which is not an integer

multiple of the period ($D = 67$ nm); therefore, gap regions and overlap regions of unmineralized collagen matrix appear alternately with an approximate ratio of 3:2 in the axial direction (Orgel et al. 2000). The detailed process of bone growth is still hotly debated (Olszta et al. 2007). Some TEM studies of embryonic bone show that the mineral nanocrystals nucleate in the gap regions and initially grow within this region (Landis et al. 1996). As the platelets grow, since they can extend the sizes of hole zones (Landis et al. 1996; Rubin et al. 2003), they may extend into the overlap regions, and, therefore, deform the collagen chain molecules. Due to the difference of the thickness of the mineral plates (2–7 nm) and collagen chain molecules (1.5 nm) (Weiner and Wagner 1998), the mineral plates cannot grow in transversely adjacent collagen gap regions (horizontal direction in Fig. 2a) and still avoid direct contact. Assuming the higher mineralized state of mature bone has similar growth mechanism as the early stage of embryonic bone, Fig. 2b shows a simplified 2-D structure model of the fully mineralized collagen fibril. Because the gap regions of the unmineralized collagen matrix are the growing centers of the mineral plates, they become the overlap regions of mineral plates in the mineralized collagen fibril, and the overlap regions of unmineralized collagen matrix become the gap regions of mineralized collagen fibril.

To show the structure more clearly, Fig. 2c is drawn to scale showing the interfaces between mineral and collagen phases. The mineral plates are staggered pattern with an axial period of 67 nm. This staggered-patterned nanocrystal-reinforced composite structure not only allows load transfer from the weak collagen matrix to the neighboring hard reinforcement mineral plates, but also optimizes the mechanical properties of the composite by utilizing the best properties of each component: high stiffness of the mineral phase and the high toughness of the collagen phase (Almer and Stock 2007; Fratzl et al. 2004; Fratzl and Weinkamer 2007). In Fig. 2c, two representative volume elements (RVEs) are highlighted, indicated by dashed boxes. These two RVEs have the same axial length (67 nm) but different distances between two neighboring plates along the radial direction. (For simplicity, the simulation work in this paper is based on only one RVE with a variable distance between neighboring plates.)

While the staggered arrangement pattern of mineral plates in the axial direction of the mineralized collagen fibril is well established, the arrangement pattern of mineral plates in the radial direction is still under debate. Originally, it was believed that the mineral plates are almost parallel along not only the axial direction, but also the other two directions (Landis et al. 1996; Traub et al. 1989). However, recent evidence shows that such a structure is only valid for a small scale including only the nearest neighboring plates (Rubin et al. 2003). At a larger scale such as the diameter of the mineralized collagen fibril, there is evidence that the collagen

molecules are assembled in a concentric pattern, as predicted by molecular simulation (Hulmes et al. 1995) and verified recently by experiment (Perumal et al. 2008). As the mineral plates nucleate and grow in the gap region of the unmineralized collagen matrix, the concentric arrangement of collagen fibrils may support a circular arrangement of mineral platelets, as proposed by Jäger and Fratzl (2000).

Because the mineralized collagen fibril is the basic building block of bone, research on the deformation mechanism at this nanoscale level is very important to fundamentally understand the excellent mechanical properties of bone. With the structure information described above, it may seem that the structure-mechanical function relationship can be easily obtained: one can use a modeling technique to create composite models representing the main structural characteristics of the bone at the mineralized collagen fibril level and calculate mechanical properties. However, there are two main obstacles that impede the understanding of bone mechanical response at this length scale. First, the complex 3-D structure of mineralized collagen fibril, especially the distribution of the mineral plates within the mineralized collagen fibril, makes it impossible to obtain an accurate analytical solution of the elastic properties of mineralized collagen fibril. Several 2-D models have been performed, but their accuracy is limited due to the various approximations involved (Gao et al. 2003; Gupta et al. 2006; Jäger and Fratzl 2000). Second, it has been difficult to obtain accurate experimental deformation data at the mineralized collagen fibril level. Thus, these early models could only compare their results to the mechanical properties of bone at the macroscopic level.

In this study, we expand upon previous models for the elastic properties of the mineralized collagen fibril in three aspects. First, we create a more detailed 3-D geometrical model to represent the structure of the mineralized collagen fibril. Second, although finite element method (FEM) is widely used in the mechanical study of bone, most of its usage is limited to the higher level of the hierarchical structure (Borah et al. 2001; Gong et al. 2007). Here, we apply FEM to study the mineralized collagen fibril level to obtain more accurate elastic properties of this smaller level structure. We also determine the stress distribution within the mineralized collagen fibril, which is not possible by using earlier analytical approaches. Third, in recent years, synchrotron X-ray measurements (particularly simultaneous wide-angle X-ray scattering (WAXS) and SAXS quantification of internal strains) have been introduced to study bone (Almer and Stock 2007; Gupta et al. 2005a). This experimental method provides crucial information on the deformation of the different phases in the mineralized collagen fibril. We use these new experimental data to verify our structural model at the fibril level and discuss the importance of different parameters in the model.

2 Modeling background

A landmark model of the mineralized collagen fibril was presented by Jäger and Fratzl (2000). Here, we briefly review their model first and then use it as a starting point to develop an improved model incorporating more structural features of the mineralized collagen fibril.

The Jäger-Fratzl model is based on a 2-D unit cell representing the mineralized collagen fibril, using periodic boundary conditions, as shown in Fig. 3 (Jäger and Fratzl 2000). This geometry is the same as the RVEs shown in Fig. 2c. In Fig. 3, the unit cell is composed of the gray rectangular inclusions representing the mineral phase and the colored continuous portions representing the collagen phase. Using this unit cell and applying periodicity and symmetry, the plate-shaped mineral reinforcement exists in a staggered

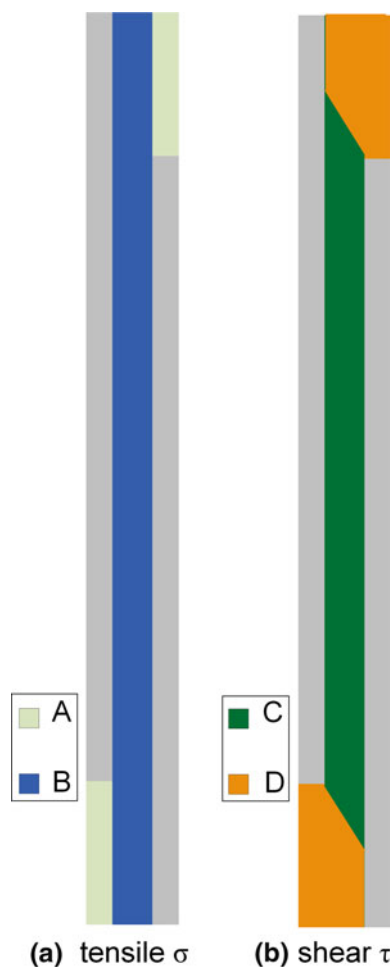


Fig. 3 Simple 2-D periodic model proposed by Jäger and Fratzl (2000) to represent the structure of the mineralized collagen fibril. Rectangular gray inclusions are the mineral phase, while colored regions are the collagen phase. The elastic behavior of the mineralized collagen fibril was approximated by dividing the collagen phase into tensile regions (region A and B) and shear regions (region C and D), while assuming the mineral phase was rigid

pattern structure: the gap region and overlap region of the mineral plates are assembled alternately. The Jäger-Fratzl model for mechanical behavior is derived by approximating the deformation behavior of the unit cell into 4 distinct regions: tensile regions (A and B) and shear regions (C and D), each with differing contributions to deformation. The elastic stress and strain values obtained from this model were much better than the results from the simple rule-of-mixtures calculation (Jäger and Fratzl 2000). However, the calculated composite modulus was still substantially overestimated—more than 200 times larger than the modulus of collagen phase (Jäger and Fratzl 2000). The ratio between the modulus of composite and the modulus of collagen phase should be about 20 (Meyers et al. 2008; Weiner and Wagner 1998). Following this original work, several other papers improved and generalized the model, but all are still confined to a 2-D structure and approximate analytic solutions (Gao et al. 2003; Gupta et al. 2005a).

One of the reasons for this large overestimation in modulus is the coarseness of the approximation—the mineral phase was assumed to be rigid (zero deformation) and the modulus of the collagen phase was taken as 50 MPa (taken from Landis et al. 1995), which is much lower than the best available estimate value (about 1 GPa) (Meyers et al. 2008). The unit cell was roughly divided into four deformation regimes as mentioned above (Jäger and Fratzl 2000), assigning larger tensile/shear deformation response to regions A/C, respectively, with scaled deformations in B and D due to the constraints of the rigid mineral phase. A simple demonstration of limitations of the assumptions of the Jäger-Fratzl analytic approach can be made here: using exactly this 2-D unit cell but with realistic stiffnesses of both phases, we perform a uniaxial deformation by FEM. We present results for compressive load instead of tensile load on the model for consistency with our later comparisons to experimental data, but note that under small elastic deformation conditions, the stress distributions are very similar between tensile and compressive loads. The results are shown in Fig. 4. From the figure, we can see that the stress/strain distribution is far more complex than the original assumption (Jäger and Fratzl 2000): neither the distribution of compressive stress/strain (analogous to tensile) (Fig. 4a, c) nor that of shear stress/strain (Fig. 4b, d) can be neatly partitioned and linearly added. Additionally, a significant stress concentration in the collagen phase near the mineral plate corner is clearly observed, which may be critical for the properties of the composite, especially the inelastic properties (Courtney 2000). Finally, the predicted ratio between the modulus of composite and the modulus of collagen phase from the new simulation is about 25, well within reasonable range (Meyers et al. 2008; Weiner and Wagner 1998). Note that the FEM analysis here lacks the smooth corners observed in natural platelets in bone (Rubin et al. 2003; Traub et al. 1989). However, the FEM results of

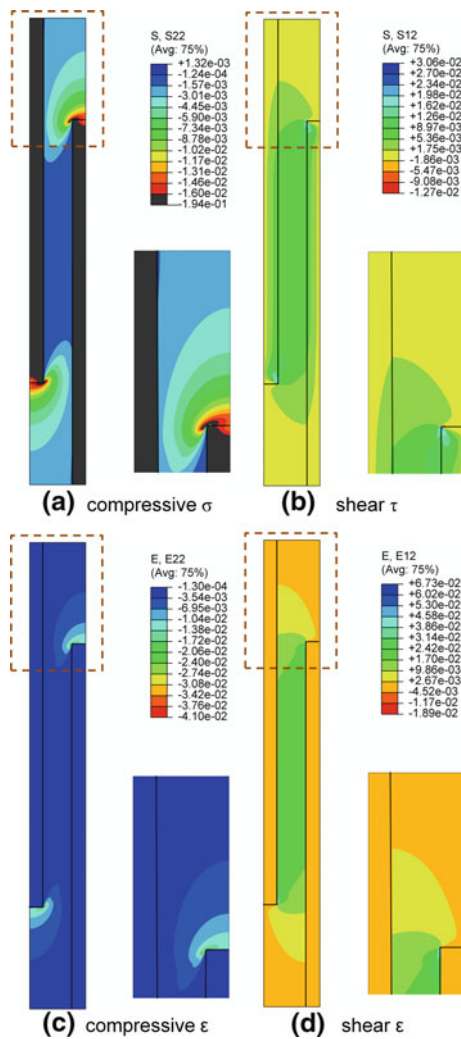


Fig. 4 The stress/strain distribution of the mineralized collagen fibril obtained by 2-D FEM: **a** compressive stress distribution (in the direction of the applied stress); **b** shear stress distribution; **c** compressive strain distribution (in the direction of the applied stress); **d** shear strain distribution. The results are calculated by using exactly the same structure as proposed by Jäger and Fratzl (2000) but with more correct properties of individual phases (1 GPa for collagen phase and 130 GPa for mineral phase) and compressive loads that are more typical instead of tensile loads. The areas within the dashed boxes are magnified on the right side for clarity to show the stress concentrations

the stress/strain distribution contour maps and overall modulus for the shapes are very similar, although the maximal stress/strain values differ due to their different stress concentration effects.

Beyond the coarse analytic approximations, an additional concern is the 2-D nature of existing models, which tend to overpredict stiffness values compared to realistic 3-D geometries (Shen et al. 2008). Therefore, in this paper, we consider a FEM implementation of several 2-D and 3-D RVE models for the mineralized collagen fibril to gain a better understanding of the deformation characteristics of this material. In the next section, our models are developed.

3 Model development

Due to the limitations of the analytical 2-D model approach to predict mineralized collagen fibril properties, we consider a numerical implementation of the 2-D model and also extensions to a more realistic 3-D representation. The 2-D models are based upon the RVE from Fig. 2c, as illustrated also in Fig. 4. All RVEs are simulated using FEM, which allows deeper understanding of the stress and strain distribution in the phases as well as easy accommodation for changes in geometry or phase properties.

3.1 3-D Geometric models

In our model, a mineralized collagen fibril is cylindrical with a diameter about 200 nm and a length about 10 μm (Craig et al. 1989; Parry and Craig 1984). In order to create an accurate 3-D RVE, we first need to consider whether the periodic boundary conditions apply. Using the above values, there are approximately 150 periods axially ($D = 67 \text{ nm}$; Rho et al. 1998) and 12 periods radially (assuming the radial period to include one plate thickness and one spacing between the plates: $4 \text{ nm} \times 2 = 8 \text{ nm}$). Therefore, the periodic boundary condition is acceptable in the axial direction (i.e., boundary effects are negligible), but must be examined carefully in the radial direction. As mentioned earlier, recent studies suggest that the mineral plates may be more likely to be in a circular pattern in the cross-section of the mineralized collagen fibril (Hulmes et al. 1995; Parry and Craig 1984). Therefore, a 3-D cylindrical collagen matrix—mineral plate composite model is created: in the axial direction, the mineral plates are parallel and in a staggered pattern with a period of 67 nm; in the radial direction, the mineral plates are arranged in a circular pattern with no plate in the central core to avoid stress concentration effects.

The staggered 3-D model is shown in Fig. 5. In the picture, because of the staggered pattern, we identify two sets of mineral plates. From the top section (Fig. 5b) and bottom section (Fig. 5c), we can see the two different sets of mineral plates separately. At the central overlap region of the mineral phase, all the mineral plates in the period appear, as shown in Fig. 5d. We can see in a small scale, especially in the outer part of the mineralized collagen fibril (the boxes in Fig. 5d), the mineral plates are almost parallel, while they are in a circular pattern in the full mineralized collagen fibril (the whole picture of Fig. 5d). This distribution is consistent with experimental observations on the mineralized tendons and potential mineral nucleation locations of unmineralized collagen fibrils (Perumal et al. 2008; Traub et al. 1989). However, as we will note in the discussion, this 3-D model is a simplified mineralized collagen fibril model and serves as a starting point of development of our approach.

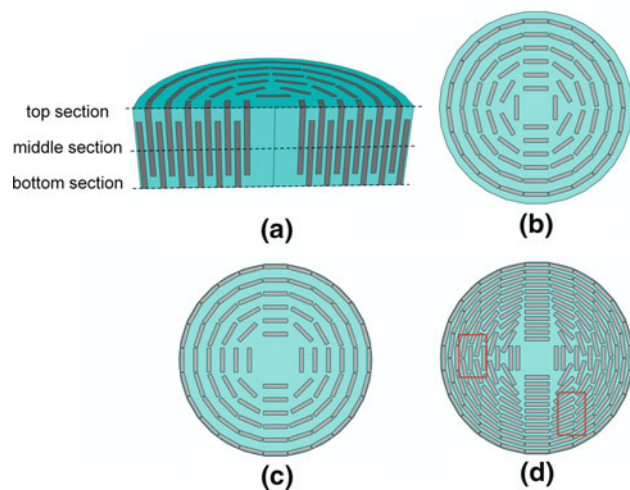


Fig. 5 Structure of the 3-D cylindrical mineralized collagen fibril FEM model (mineral phases are shown in *gray* color). **a** Half-cut view of the mineralized collagen fibril cut along the lateral direction, showing the staggered pattern which can be divided into two sets of mineral plates; **b** top section and **c** bottom section of the mineralized collagen fibril, showing the different sets of mineral plates that are in the gap regions of the mineral phase separately; **d** middle section of the mineralized collagen fibril, showing the overlap region of the mineral phase. The mineral plates in the mineralized collagen fibril form a circular pattern, while at the smaller scale, they are almost parallel with the neighboring ones. The mineral plates are distributed more densely in the outer part of the mineralized collagen fibril

3.2 FEM implementation

In this paper, we consider both the two- and three-dimensional RVEs of the mineralized collagen fibril in a FEM simulation using the software ABAQUS. In the 2-D model, geometry from Fig. 2c (and Fig. 4), a biased mesh is used to obtain finer mesh at the corners to appropriately capture the stress concentration near the mineral plate corners. Both 2-D and 3-D models are meshed using quadratic elements and solved via the ABAQUS standard scheme. Sample meshes are shown in Fig. 6. The boundary conditions of the composite assume that the mineralized collagen fibril maintains its cylindrical shape (or in 2-D case, rectangular shape) during elastic loading, i.e., constant displacement in the axial direction along the top surface and bottom surface due to the periodicity along this direction and a uniform displacement in the radial direction for all nodes on the outer surface of mineralized collagen fibril. From the simulation results, the overall elastic Young's modulus and local stress fields of the composite and its phases are calculated, for various material properties and micro-geometries.

3.3 Material parameters

There is a wide range of parameter values connecting the structure of the mineralized collagen fibril for bones from

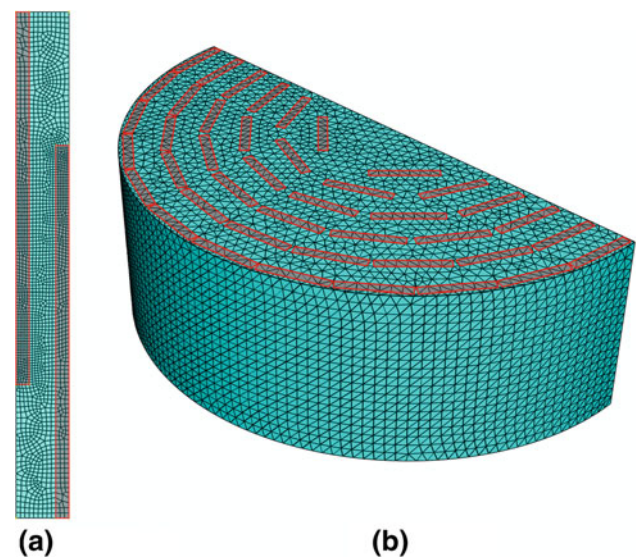


Fig. 6 Mesh samples of the FEM model used in ABAQUS. **a** 2-D models; **b** 3-D models (The *red outlined regions* indicate the location of the mineral plates)

different animals or from different anatomical locations within a given animal. Due to the periodicity of our model in the axial direction, the length of the model is constant at 67 nm. From the literature, there are wide ranges for the other structural parameters: the radius of the mineralized collagen fibril is 40–150 nm, the mineral plates are 15–150 nm in length, 10–80 nm in width and 2–7 nm in thickness, and the distance between the neighboring plates is on the same order of the thickness (Lowenstam and Weiner 1989; Rubin et al. 2003). To focus on the effects of the size of the mineral plates, we fix the radius of the mineralized collagen fibril as 100 nm. To further reduce the complexity, we use the most commonly cited value of 25 nm for the width of the mineral plates (Lowenstam and Weiner 1989), leaving the other two dimensions as variables. Therefore, three structural parameters remain to be specified—the thickness of the mineral plates, the length of the mineral plates and the spacing between them. These parameters are linked by the volume fraction of the mineral phase, which is an important characteristic of bone and can be relatively easily measured through various methods, for example, thermogravimetric analysis (TGA) (Lozano et al. 2003). The volume fraction of the mineral phase can also be calculated from the geometric structure as the total volume of the mineral plates divided by the volume of the collagen matrix cylinder; therefore, we use the volume fraction to replace one of the above parameters, and we choose the length of the mineral plates here. To study geometric effects, here, we discuss the most common range of these three parameters: plate thickness between 3 and 4.5 nm, distance between the plates between 2 and 4.5 nm and volume fraction between 30 and 48% (Lowenstam and Weiner 1989).

In addition to the structural parameters, the intrinsic properties of the two phases are also variables in our model. For the elastic properties of interest here, the most important values are the Young's moduli and Poisson's ratios of the two phases. Poisson's ratios of mineral and collagen phases are reported as 0.28 (Gilmore and Katz 1982, deduced from the measurements of elastic wave velocities) and 0.25 (Akiva et al. 1998; Jäger and Fratzl 2000, the "effective" value that simplifies nonlinear and anisotropic properties of collagen), respectively. For Young's modulus of the mineral phase, values are typically cited within the range between 100 and 150 GPa (Gilmore and Katz 1982; Koch et al. 2007). It is noted that all these values are measured from artificial bulk crystalline hydroxyapatite samples. The difference between these values (Gilmore and Katz 1982; Koch et al. 2007; Vincent 1990) and the modulus value for the natural mineral nanoplates in bone will be discussed later. For the Young's modulus of collagen phase, literature reports a range from 0.8 to 1.5 GPa (Gupta et al. 2005b; Heim et al. 2006; Meyers et al. 2008).

In addition to the three structural and two material property parameters, the effect of approximations to the morphology is also considered. Considering different structural complexities are very important, as it provides insight to the evolution of the complex, hierarchical structure, as well as indicates the level of refinement of the model required for predictive accuracy. Four RVEs are selected (seen in Fig. 7): (a) a simple 2-D periodic structure; (b) 2-D half-symmetric structure (still 2-D but without the periodic boundary condition in radial direction); (c) 3-D axial symmetric structure (extending the structure (b) to 3-D but considering the mineral phase as a continuous cylindrical annuli, without discretizing the plates) and (d) the 3-D complex model illustrated in Fig. 5.

3.4 Calculation of elastic properties

This study focuses on the elastic behavior of the mineralized collagen fibril, therefore small loads are applied in the FEM model, excluding plasticity in both phases and bond rupture or relative sliding on the interface between two phases.

To investigate how the elastic properties of the mineralized collagen fibril depend on the structural and material parameters mentioned previously, we choose two target values for the simulation. These are the apparent moduli of the collagen phase and the mineral phase, which are defined as the total applied stress σ_{app} divided by the average strain in the collagen phase $\bar{\varepsilon}_{\text{coll}}$ and in the mineral phase $\bar{\varepsilon}_{\text{min}}$, respectively, i.e.,

$$E_{\text{collagen}}^{\text{apparent}} = \sigma_{\text{app}} / \bar{\varepsilon}_{\text{coll}} \quad (1)$$

$$E_{\text{mineral}}^{\text{apparent}} = \sigma_{\text{app}} / \bar{\varepsilon}_{\text{min}} \quad (2)$$

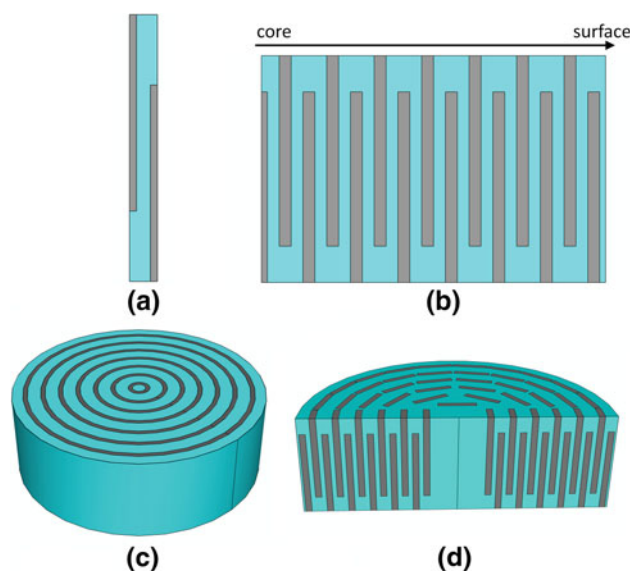


Fig. 7 Four RVEs used to approximate the mineralized collagen fibril geometry (mineral phases are shown in gray color): **a** 2-D periodic structure (as in the Jäger and Fratzl 2000); **b** 2-D half-symmetric structure (with the consideration of boundary effect in radial direction); **c** 3-D axial symmetric structure (extending the structure **b** to 3-D but without considering individual platelets for the mineral phase); **d** the 3-D complex model (as also illustrated in Fig. 5)

These two target values are chosen so that the simulation can be compared directly with values measured from the synchrotron X-ray scattering experiments, which report average strains in the collagen phase (by SAXS) and in the mineral phase (by WAXS) (Almer and Stock 2007; Gupta et al. 2005a). Thus we will use E_{SAXS} and E_{WAXS} to represent the apparent moduli of collagen phase and mineral phase, respectively. These apparent moduli naturally differ from the moduli of the respective pure materials, as they account for the interaction between two phases. Therefore, $E_{\text{collagen}}^{\text{apparent}}$ is much larger than the modulus of pure collagen while $E_{\text{mineral}}^{\text{apparent}}$ is smaller than the modulus of pure hydroxyapatite, as shown later in the Sect. 4.

The average strain in the collagen phase represents the deformation within the axial distance between one mineral plate and the neighboring one, which is approximately 67 nm. In our model, this distance is BE in Fig. 8a (using the 2-D periodic diagram for clarity). Because of symmetry, the deformation in region AB is the same as region DE; therefore, we can use deformation of the region AD to calculate the average strain in the collagen phase. The average strain in the mineral phase measured by the experiment is the average strain of the mineral lattice, which is equal to the average strain of the mineral plates, which is region BF in Fig. 8a. Again, because of the symmetry, we can calculate deformation in region BD instead of BF. Therefore, the apparent moduli in both phases can be calculated in one period of the mineralized collagen fibril (the upper half region AD in Fig. 8a with $D = 67$ nm).

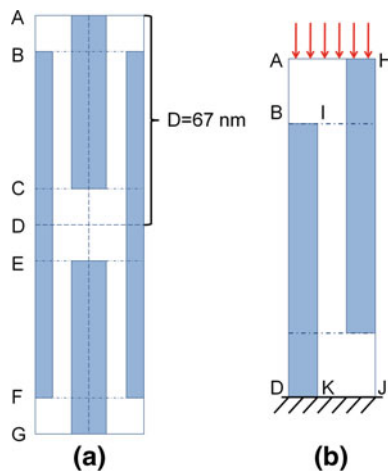


Fig. 8 2-D periodic sketch showing the regions in the model corresponding to SAXS and WAXS measurement. **a** Due to the periodic boundary condition, the simulation can be processed in one period—the deformation within region AD is used for E_{SAXS} and deformation within region BD is used for E_{WAXS} . **b** Within one period, the periodic boundary condition can make the calculation even simpler—lower surface DJ is fixed, the average displacements of surfaces AH and BI are sufficient

Figure 8b shows the model reduced to only one period, and this is the same as the model we use here for the simplest 2D FEM simulation. Because of the periodic and symmetric boundary condition in the axial direction, all points on the upper surface AH have the same displacement, and surface DJ is fixed. Therefore, for the small deformation within the elastic range, the strain in the collagen phase can be calculated as displacement of surface AH (d_{AH}) divided by the length between AH and DJ (l_{AD}), which is equal to the period 67nm. Similarly, to obtain the average strain in the mineral phase, only the average displacement of the surface BI (d_{BI}) after loading is required, divided by the original length between BI and DK (l_{BD}). Thus, the equations to calculate the E_{SAXS} and E_{WAXS} from the FEM model are as follows:

$$E_{\text{collagen}}^{\text{apparent}} = E_{SAXS} = \sigma_{\text{app}} / (d_{AH} / l_{AD}) \quad (3)$$

$$E_{\text{mineral}}^{\text{apparent}} = E_{WAXS} = \sigma_{\text{app}} / (d_{BI} / l_{BD}) \quad (4)$$

Table 1 Parameter ranges used in predictions by the mineralized collagen fibril models to determine the elastic properties (Lowenstam and Weiner 1989)

Parameter	Structure	E_{collagen} (GPa)	E_{mineral} (GPa)	Volume fraction	Distance of mineral plates (nm)	Thickness of mineral plates (nm)
Range	4 RVEs	0.8–1.5	100–150	30–48%	2–4.5	3–4.5
Standard value	2-D periodic	1	130	42%	3.5	3.5
CV_{collagen}	0.0254	0.115	0.0971	0.333	0.0338	0.112
CV_{mineral}	0.0309	0.00418	0.172	0.192	0.00583	0.00172

Coefficients of the variation (CV) are also shown for the predicted moduli under change of each individual parameter within its range

We note that Eq. 4 gives results identical to those obtained by integrating the strains element by element, e.g.

$$E_{WAXS} = \sigma_{\text{app}} \left(\frac{\sum_i \varepsilon_i}{N_i} \right)^{-1} \quad (5)$$

where i sums over all elements in BKDI and N_i is the number of elements in BKDI. Therefore, we use Eqs. 3 and 4 in the later study for simplicity.

4 Results

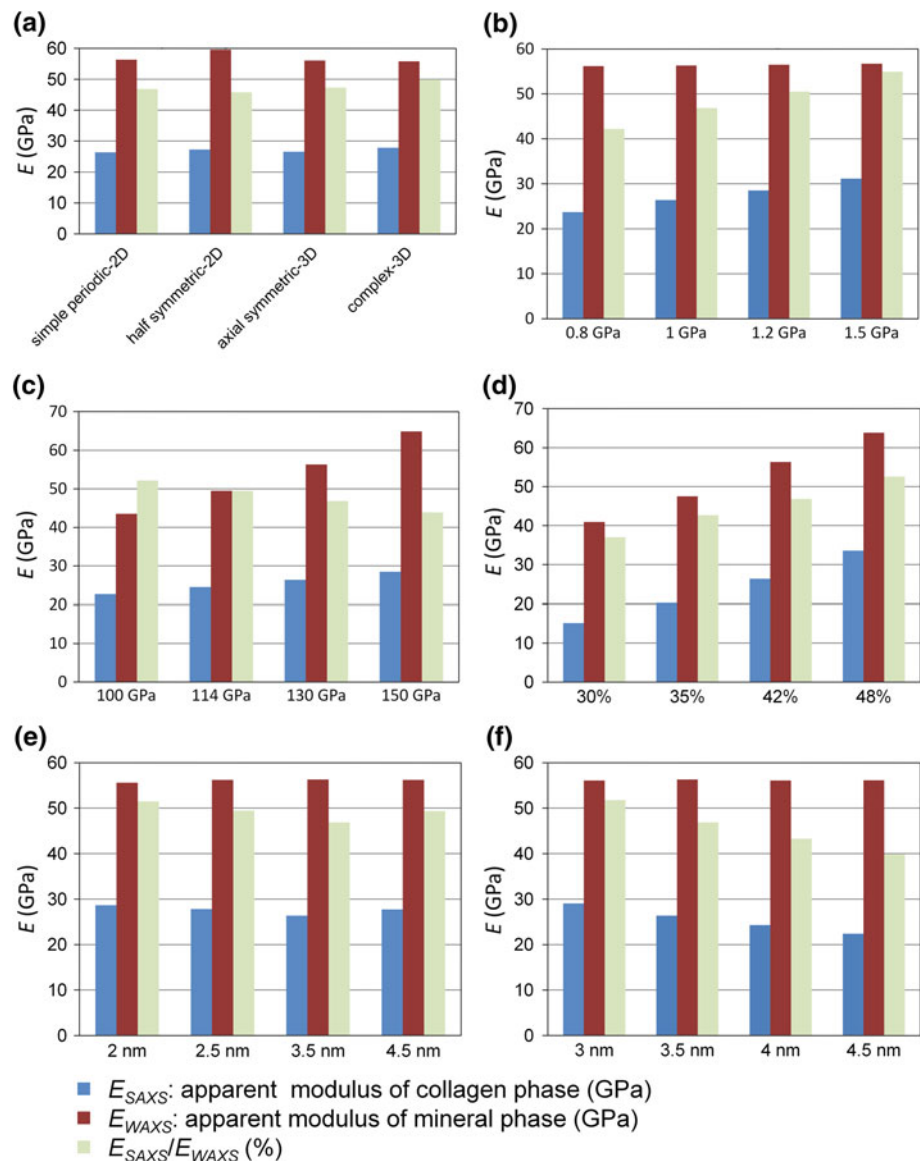
In this section, we report FEM simulations of the four different structural representations of the mineralized collagen fibril (shown in Fig. 7), considering variation in the material parameters. Results are also validated against experimental data.

4.1 Parametric study

The values of the apparent moduli of the collagen and mineral phases are calculated to show the dependence of the elastic properties of the mineralized collagen fibril on the parameters within the ranges mentioned previously. Only one variable is considered at a time, assuming that the interactions between the parameters are negligible within the ranges considered. The range and standard parameter values are shown in Table 1 (Lowenstam and Weiner 1989). To show the influence of each parameter on the elastic properties of the mineralized collagen fibril, we choose four values for each parameter while holding the other parameters constant at their standard values and calculate the values of the apparent moduli of collagen phase and mineral phase.

For the four structural models of the mineralized collagen fibril (Fig. 7), the calculated apparent moduli are shown in Fig. 9. From Fig. 9a and the values of the coefficients of the variation (CV) listed in Table 1, which are defined as the standard deviation of the predicted values divided by the average of those values as the parameter is varied, surprisingly we find very little influence on apparent moduli when we change the complexity of the structure, the level of

Fig. 9 Dependence of apparent moduli of the collagen phase E_{SAXS} and mineral phase E_{WAXS} on material and structural parameters. Predicted apparent moduli as a function of **a** complexity of structure (level of structural detail contained in the RVE); **b** Young's modulus of collagen phase; **c** Young's modulus of mineral phase; **d** volume fraction of mineral phase; **e** distance between mineral plates; **f** thickness of mineral plates



structural detail in the RVE. However, the present calculation is limited to the elastic properties of bone at the mineralized collagen fibril level; the influence of the complex structure may be more important in the time-dependent mechanical properties of bone (Puxkandl et al. 2002) and in larger scale deformations.

Because increasing the structural complexity of the RVE does not lead to significant changes in the predicted apparent phase moduli, the 2-D periodic structure is used for the remaining simulations to optimize the modeling efficiency. The CV values for different varying parameters are shown in Table 1.

From the results in Fig. 9 and Table 1, we conclude that (1) the complexity of the structure and the distance between the mineral plates are not critical parameters for either apparent modulus while the volume fraction of the mineral phase is

the most influential parameter; (2) except for changes in the Young's modulus of the mineral phase, the apparent modulus of the mineral phase is less sensitive to parameter changes than the apparent modulus of the collagen phase: the Young's modulus of the collagen phase and the thickness of the mineral plates even do not contribute significantly to E_{WAXS} changes; (3) for the appreciable changes, the apparent moduli monotonically increase as the parameter values increase, except for an inverse relationship between apparent modulus of collagen phase and the thickness of the mineral plates.

4.2 Model validation

To verify our mineralized collagen fibril model, we compare our simulation results with experimental data obtained from SAXS and WAXS measurements on a sample of canine

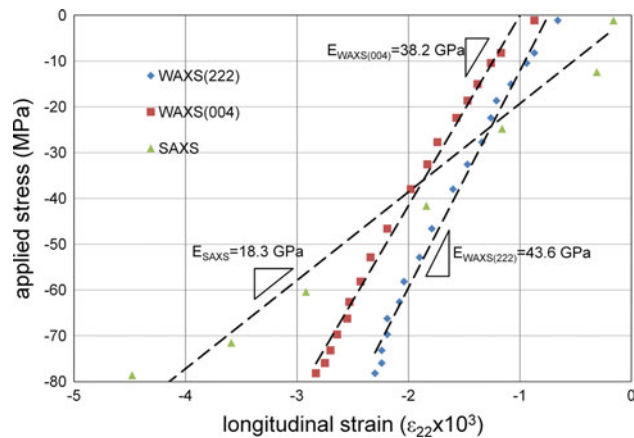


Fig. 10 Average strains measured in mineral phase (from 00.4 and 22.2 reflections, WAXS) and in collagen phase (D-period, SAXS) as a function of applied stress on a sample from a canine fibula. Slopes are the apparent moduli of each phase (data from Fig. 2 in Almer and Stock 2007)

fibula (Almer and Stock 2007). The relevant data are plotted in Fig. 10, where the slopes of the lines represent the corresponding apparent phase moduli. Because the structural details of this particular canine fibula sample at the nanostructure level are uncertain, we make the following assumptions: we use the average values (for structural parameters, except volume fraction of mineral plates) or the most accepted values (for elastic property parameters) as the standard values here. These values are the same as the standard values in Table 1, with the exception that we use both the 2-D simple periodic and 3-D complex structural models (seen in Fig. 7) and use 114 GPa as Young's modulus of mineral phase (Gilmore and Katz 1982). Therefore, the only undecided parameter is the volume fraction of the mineral phase.

Because the volume fraction of the mineral phase is the most important factor for the elastic properties of the mineralized collagen fibril as shown earlier, we measured this parameter using the TGA technique in a Mettler Toledo TGA/SDTA 851^e Thermogravimetric Analyzer. The measurement was performed on three small samples that were cut from the different locations of the same fibula which are near the synchrotron X-ray data gathering area. The weight of the samples ranged from 3 to 7 mg and samples were heated from 25 to 650°C at a rate of 10°C/min. After reaching 650°C, temperature was held constant for 5 min. The weight fraction of water

and collagen were determined from the accumulated weight loss between 20 and 225°C and between 225 and 650°C, respectively, and converted to volume fraction by using densities of 1 g/cm³ for water, 3.153 g/cm³ for hydroxyapatite and 1.343 g/cm³ for collagen (Fels 1964; Hoffmann et al. 2003). Assuming all the mineral phase is in the mineralized collagen fibril (extra-fibrillar mineral phase is discussed later), the volume fraction of the mineral phase in the mineralized collagen fibril obtained from the TGA measurement is 36.8%, which is then used in the FEM simulation with 2-D simple periodic and 3-D complex structural models (Fig. 7).

The detailed results comparing the experimental results, using a mineral phase volume fraction of 36.8%, are listed in Table 2. It is apparent that the 2-D simple periodic and the 3-D complex simulation values are both very close to the experimental values. Possible explanations for the differences will be discussed further in the next section. From Fig. 10, it is clear that the mineral phase has approximately 0.1% residual strain in the unstressed state (Almer and Stock 2007). To determine if this residual strain has an impact on the modulus data, a residual strain is introduced into the simulation by a pre-deformation of the mineral beyond its elastic limit such that upon unloading the residual strain of the mineral is 0.1%. Using a model with pre-deformed mineral plates, the simulations are re-run to obtain new values of E_{SAXS} and E_{WAXS} . The results shown in Table 2 are very similar to those without residual strain. This result is encouraging because studies show that while residual strain in bone may influence the strength of bone, it has little impact on its stiffness (Almer and Stock 2007). With the reasonable match of apparent phase moduli values in both prestrained and unprestrained conditions, the proposed mineralized collagen fibril models based on a finite element RVE structure satisfactorily captures the elastic properties at the nano-scale.

5 Discussion

In the previous section, the simulation of elastic properties with the finite element RVE models provided satisfactory agreement with experimental data. However, these results are based on three major simplifications: (1) the modulus of

Table 2 Comparison of elastic properties between experimental results (Almer and Stock 2007) and simulation results

	Prestrain	E_{SAXS} (GPa)	E_{WAXS} (GPa)	E_{SAXS}/E_{WAXS}
Experiment	0.1%	18.3	40.9 ^a	0.447
Simulation-2D	0	19.1	40.6	0.470
Simulation-2D	0.1%	19.2	40.6	0.473
Simulation-3D	0	20.5	43.7	0.469
Simulation-3D	0.1%	20.5	43.7	0.469

^a Average value using (004) and (222) reflections

the mineral phase is assumed to be the same as that measured on bulk crystalline hydroxyapatite, (2) the water and collagen phases are combined into a single matrix phase, and (3) the higher hierarchical levels of bone structure are ignored. Here, we will discuss the effect of water on the elastic properties of mineralized collagen fibril and how the difference between the properties of bulk hydroxyapatite and natural hydroxyapatite as found in bone could influence the elastic properties of mineralized collagen fibril. Finally, the influence of the other structural complexities including higher hierarchical levels on the elastic properties of mineralized collagen fibril is discussed and the methods for implementation are suggested.

5.1 Mineral modulus effect

In the above work, we use elastic properties of the mineral phase obtained from measurements on bulk single crystal hydroxyapatite: bulk single crystal hydroxyapatite is nearly isotropic, with a modulus of 114 GPa and Poisson's ratio of 0.28 (Gilmore and Katz 1982). Although these values are widely accepted in the bone modeling community and are often used to represent the elastic properties of the mineral phase in the mineralized collagen fibril, the nanocrystalline form of the mineral phase in the mineralized collagen fibril is significantly different from the bulk single crystal hydroxyapatite.

The mineral plates in natural mineralized collagen fibrils are very thin, with thicknesses in most cases <5 nm. Such narrow plates imply that these nanocrystals are only eight crystal lattices at most in the thickness direction of the mineral plate (Jokanovic et al. 2006). The resulting very large surface area to volume ratio in these nanoplates indicates that the interface layers between mineral plate and collagen might play an important role in the mechanical properties. Because the perfect periodic array of the crystal lattice is truncated at the interface, the resulting surface reconstruction can propagate several interfacial atomic layers into the solid and change the original bonding status from that of the bulk material, thus changing the elastic properties of the nanoplate (Chen et al. 2006; Cuenot et al. 2004). Therefore, the mineral plates in bone can potentially be viewed as a core-shell structure—the outside shell is the reconstructed lattice structure and the inner core is composed of a perfect crystal lattice structure which has the same properties as the corresponding bulk material.

TEM studies showed that the outer layer of the mineral plates consists of amorphous domains of mineral (Olszta et al. 2007; Rho et al. 1998) and that the thickness of the amorphous layer in the mineral phase could be about 1 nm (Bertinetti et al. 2007). For mineral plates with a thickness of 3.5 nm (standard value in Table 1), the volume fraction of the amorphous phase could therefore be as much as 60%.

The existence of amorphous hydroxyapatite may lower the average modulus of the mineral plate, because the Young's modulus of amorphous hydroxyapatite is significantly less than that of the fully crystalline phase; one study measured a value of 80 GPa for amorphous hydroxyapatite (Koch et al. 2007). Employing the rule of mixtures (isostrain condition) to simply evaluate the modulus of such a core-shell structured mineral phase, the overall modulus for the mineral plate would be lowered to 95 GPa. 3-D simulations performed using this lower value for the modulus of the mineral phase yields apparent moduli of 19.8 and 39.6 GPa for E_{SAXS} and E_{WAXS} , respectively. These values are even closer to the experimentally measured values in Table 2, indicating that this mechanism may be important to capture in the simulations.

5.2 Water effect

Water is the third major component in bone and occupies about 10–25% of the bone mass (Currey 2003). The TGA results show that the average weight fraction of water is 12.9% in our canine fibula samples. Water in bone may exist in three different forms: free water in pores, bound water in the collagen network (including collagen-mineral interface) and tightly bound water in the mineral phase (Wang and Puram 2004). The free water in the pores of cancellous bone is outside the scale of study (cortical bone in nanoscale), so the free water portion is not relevant for this study. Water in the mineral phase is tightly bound and exists at relatively low percentage and thus can also be neglected (Lowenstam and Weiner 1989). However, the bound water in the collagen network may have significant influence on its nanoscale Young's modulus. Because the current model does not account for fluid-solid interaction, the water phase and the collagen phase are combined together into a single matrix collagen phase in our model and the Young's modulus of this phase is taken as that of wet collagen matrix (Heim et al. 2006; Meyers et al. 2008).

We note that the importance of water to determine mechanical properties of bone: bones with different water content display obvious differences in stiffness and strength (Nyman et al. 2006; Smith and Walmsley 1959). Moreover, to describe the time-dependent mechanical behavior of bone, i.e., creep or fatigue, the contribution of the bound water should be considered more carefully on several grounds: first, the bound water in the collagen network will change the viscoelasticity of collagen phase dramatically (Sasaki and Enyo 1995; Yamashita et al. 2001); second, the bound water on the mineral-collagen interface will change the interfacial bonding properties (Knowles et al. 2007); third, water may migrate and change its local distribution within the collagen matrix in response to stress localization, consequently introducing the non-uniform properties into the collagen phase.

5.3 Additional structure complexities

In this study, we have focused on the elastic properties of the mineralized collagen fibril and simplified bone as a two-phase composite—mineral nanoplates aligned within a collagen matrix. However, here we excluded two structural complexities of bone which should be considered in studies of more complex deformation: debonding of the collagen-platelet interface and interfibrillar mineral.

First, as shown in the preliminary FEM results (Fig. 4), significant stress concentration exists around the interface between the mineral phase and collagen phase, which could induce debonding on the interface. Some preliminary studies in this group show that the interfacial properties play an important role for the time-dependent mechanical properties of bone. In the context of this paper, to understand how the bond rupture could influence the elastic properties of mineralized collagen fibril, a static-kinetic friction method was introduced into the model to simulate the perfect bonding—debonding—rebonding process of the mineral-collagen interface under loading (Knowles et al. 2007): initially at small loads, the two phases are perfectly bonded; as the stress increases, the kinetic friction criterion is satisfied and interfacial bond rupture and sliding occurs; and finally, during the unloading phase, the sliding ceases and ruptured interfacial bonds rebond. By using this method, the apparent moduli of two phases were recalculated. The results (from 2-D periodic model) show that both elastic moduli change very little (<1%), indicating that interface bond rupture can be ignored for the current study. However, this conclusion is limited to the elastic properties of the mineralized collagen fibril.

Second, as mentioned in the introduction, bone structure is hierarchical and has different structures at different length scales. At next structural level (mineralized collagen fibril bundle), mineralized collagen fibrils are almost always arranged in arrays aligned along collagen fibrils' axial direction (Reid 1987; Weiner and Wagner 1998). Between these mineralized collagen fibrils, there are proteoglycans and other proteins formed as a matrix, which interconnect the discrete mineralized collagen fibrils and assembles them into mineralized collagen fibril arrays (Fratzl 2003; Puxkandl et al. 2002). Importantly, mineral plates also form on the surface of the mineralized collagen fibrils and in the interfibrillar space (Olszta et al. 2007). These mineral nanocrystals are called interfibrillar mineral. At least about 15% of total mineral phase is believed to be of the interfibrillar type (Martin et al. 1998). Therefore, the actual amount of the mineral inside the mineralized collagen fibril is smaller than the TGA-measured total volume fraction of mineral phase of bone.

To understand how the inclusion of interfibrillar mineral content will influence the properties of microscopic bone (in

the order of synchrotron X-ray measurement area—about 50 by 50 μm), the current mineralized collagen fibril model should be extended to a larger scale. A simple and possible way to further this study is to use a bottom-up modeling method: creation of a three-phase composite: the proteoglycan-rich proteinous matrix reinforced by aligned mineralized collagen fibrils and distributed interfibrillar mineral.

6 Conclusions

The fundamental understanding of the mechanical behavior of bone relies on a thorough understanding of the behavior of the mineralized collagen fibrils, which are the basic building block of bone. This article focuses on the relationship between the structure and elastic properties of mineralized collagen fibril. Two- and three-dimensional FEM models are created to represent the main structural characteristics of mineralized collagen fibril, consisting of nano-scale hydroxyapatite plates aligned in a collagen matrix, in a RVE approach. By using FEM to simulate the mechanical response of this model, we assess how major structural and material properties parameters influence the elastic behavior of the mineralized collagen fibril. The modeling results are compared with published experimental data obtained by synchrotron X-ray scattering technique, which measure the spatially averaged apparent moduli of the collagen phase and the mineral plates separately. The computational and experimental results agree well, indicating the strength of this numerical RVE approach. An important finding is that a 2-D RVE model is sufficient to understand elastic properties. However the RVE must appropriately account for phase morphology and accurately assess load transfer between phases, as is accomplished in our simple 2-D unit cell simulated in FEM. It was found that the most important parameter governing stiffness is the volume fraction of the mineral phase, when considering parameter variations within the physically valid ranges. Finally, the implications of partial amorphization of the hydroxyapatite mineral plates are considered and the effect of water on the elastic behavior of the mineralized collagen fibril is discussed. The limitation of the current model due to the exclusion of interfibrillar mineral content is noted and future work is warranted to examine this issue as well as interfacial bonding for elastic and inelastic deformations.

Acknowledgments We thank Ms. A. C. Deymier-Black for assistance with TGA measurement. We also thank Ms. A. Singhal and Ms. A. C. Deymier-Black for their invaluable assistance and discussions about the structure and mechanical properties of the mineralized collagen fibril. This study is financially supported by the U.S. Department of Energy, Office of Science, Office of Basic Energy Sciences, under Contract No. DE-AC02-06CH11357.

References

- Akiva U, Wagner HD, Weiner S (1998) Modelling the three-dimensional elastic constants of parallel-fibred and lamellar bone. *J Mater Sci* 33:1497–1509
- Almer JD, Stock SR (2007) Micromechanical response of mineral and collagen phases in bone. *J Struct Biol* 157: 365–370. doi:10.1016/j.jsb.2006.09.001
- Ashby MF (1993) Criteria for selecting the components of composites. *Acta Metall Mater* 41:1313–1335
- Bertinetti L, Tampieri A, Landi E, Ducati C, Midgley PA, Coluccia S, Martra G (2007) Surface structure, hydration, and cationic sites of nanohydroxyapatite: UHR-TEM, IR, and microgravimetric studies. *J Phys Chem C* 111: 4027–4035. doi:10.1021/jp066040s
- Birk DE, Silver FH, Trelstad RL (1991) Matrix Assembly. In: Hay ED (ed) *Cell biology of extracellular matrix*. Plenum, New York pp 221–254
- Borah B, Gross GJ, Dufresne TE, Smith TS, Cockman MD, Chmielewski PA, Lundy MW, Hartke JR, Sod EW (2001) Three-dimensional microimaging (MR μ I and μ CT), finite element modeling, and rapid prototyping provide unique insights into bone architecture in osteoporosis. *Anat Rec* 265:101–110
- Chen CQ, Shi Y, Zhang YS, Zhu J, Yan YJ (2006) Size dependence of Young's modulus in ZnO nanowires. *Phys Rev Lett* 96:075505. doi:10.1103/PhysRevLett.96.075505
- Courtney TH (2000) *Mechanical behavior of materials*, 2edn. McGraw Hill, Boston
- Craig AS, Birtles MJ, Conway JF, Parry DAD (1989) An estimate of the mean length of collagen fibrils in rat tail-tendon as a function of age. *Connect Tissue Res* 19:51–62
- Cuenot S, Fretigny C, Demoustier-Champagne S, Nysten B (2004) Surface tension effect on the mechanical properties of nanomaterials measured by atomic force microscopy. *Phys Rev B* 69:165410. doi:10.1103/PhysRevB.69.165410
- Currey JD (2003) Role of collagen and other organics in the mechanical properties of bone. *Osteoporos Int* 14:S29–S36. doi:10.1007/s00198-003-1470-8
- Delmas PD, Tracy RP, Riggs BL, Mann KG (1984) Identification of the noncollagenous proteins of bovine bone by two-dimensional gel-electrophoresis. *Calcif Tissue Int* 36:308–316
- Dorozhkin SV, Epple M (2002) Biological and medical significance of calcium phosphates. *Angew Chem Int Edit* 41:3130–3146
- Fels IG (1964) Hydration and density of collagen and gelatin. *J Appl Polym Sci* 8:1813–1824
- Fratzl P (2003) Cellulose and collagen: from fibres to tissues. *Curr Opin Colloid Interface Sci* 8: 32–39. doi:10.1016/S1359-0294(03)00011-6
- Fratzl P, Gupta HS, Paschalis EP, Roschger P (2004) Structure and mechanical quality of the collagen-mineral nano-composite in bone. *J Mater Chem* 14:2115–2123. doi:10.1039/b402005g
- Fratzl P, Weinkamer R (2007) Nature's hierarchical materials. *Prog Mater Sci* 52:1263–1334. doi:10.1016/j.pmatsci.2007.06.001
- Gao HJ, Ji BH, Jäger IL, Artz E, Fratzl P (2003) Materials become insensitive to flaws at nanoscale: lessons from nature. *Proc Natl Acad Sci USA* 100:5597–5600. doi:10.1073/pnas.0631609100
- Gilmore RS, Katz JL (1982) Elastic properties of apatites. *J Mater Sci* 17:1131–1141
- Gong H, Zhang M, Qin L, Hou YJ (2007) Regional variations in the apparent and tissue-level mechanical parameters of vertebral trabecular bone with aging using micro-finite element analysis. *Ann Biomed Eng* 35:1622–1631. doi:10.1007/s10439-007-9332-8
- Gupta HS, Schratzer S, Tesch W, Roschger P, Berzlanovich A, Schoeberl T, Klaushofer K, Fratzl P (2005) Two different correlations between nanoindentation modulus and mineral content in the bone-cartilage interface. *J Struct Biol* 149:138–148. doi:10.1016/j.jsb.2004.10.010
- Gupta HS, Seto J, Wagermaier W, Zaslansky P, Boesecke P, Fratzl P (2006) Cooperative deformation of mineral and collagen in bone at the nanoscale. *Proc Natl Acad Sci USA* 103:17741–17746. doi:10.1073/pnas.0604237103
- Gupta HS, Wagermaier W, Zickler GA, Aroush DRB, Funari SS, Roschger P, Wagner HD, Fratzl P (2005) Nanoscale deformation mechanisms in bone. *Nano Lett* 5:2108–2111. doi:10.1021/nl051584b
- Hassenkam T, Fantner GE, Cutroni JA, Weaver JC, Morse DE, Hansma PK (2004) High-resolution AFM imaging of intact and fractured trabecular bone. *Bone* 35:4–10. doi:10.1016/j.bone.2004.02.024
- Heim AJ, Matthews WG, Koob TJ (2006) Determination of the elastic modulus of native collagen fibrils via radial indentation. *Appl Phys Lett* 89:181902. doi:10.1063/1.2367660
- Hoffmann U, Kwait DC, Handwerker J, Chan R, Lamuraglia G, Brady TJ (2003) Vascular calcification in ex vivo carotid specimens: precision and accuracy of measurements with multi-detector row CT. *Radiology* 229:375–381. doi:10.1148/radiol.2292021016
- Hulmes DJS (2002) Building collagen molecules, fibrils, and supra-fibrillar structures. *J Struct Biol* 137:2–10. doi:10.1006/jsbi.2002.4450
- Hulmes DJS, Wess TJ, Prockop DJ, Fratzl P (1995) Radial packing, order, and disorder in collagen fibrils. *Biophys J* 68:1661–1670
- Jäger I, Fratzl P (2000) Mineralized collagen fibrils: a mechanical model with a staggered arrangement of mineral particles. *Biophys J* 79:1737–1746
- Jokanovic V, Izvonar D, Dramicanin MD, Jokanovic B, Zivojinovic V, Markovic D, Dacic B (2006) Hydrothermal synthesis and nanostructure of carbonated calcium hydroxyapatite. *J Mater Sci Mater Med* 17:539–546. doi:10.1007/s10856-006-8937-z
- Knowles TP, Fitzpatrick AW, Meehan S, Mott HR, Vendruscolo M, Dobson CM, Welland ME (2007) Role of intermolecular forces in defining material properties of protein nanofibrils. *Science* 318:1900–1903. doi:10.1126/science.1150057
- Koch CF, Johnson S, Kumar D, Jelinek M, Chrisey DB, Doraiswamy A, Jin C, Narayan RJ, Millalelescu IN (2007) Pulsed laser deposition of hydroxyapatite thin films. *Mater Sci Eng C Biomimetic Supramol Syst* 27:484–494. doi:10.1016/j.msec.2006.05.025
- Landis WJ, Hodgins KJ, Arena J, Song MJ, McEwen BF (1996) Structural relations between collagen and mineral in bone as determined by high voltage electron microscopic tomography. *Microsc Res Tech* 33:192–202
- Landis WJ, Librizzi JJ, Dunn MG, Silver FH (1995) A study of the relationship between mineral content and mechanical properties of turkey gastrocnemius tendon. *J Bone Miner Res* 10:859–867
- Lowenstam HA, Weiner S (1989) *On Biomineralization*. Oxford University, New York
- Lozano LF, Pena-Rico MA, Heredia A, Octolan-Flores J, Gomez-Cortés A, Velázquez R, Belio IA, Bucio L (2003) Thermal analysis study of human bone. *J Mater Sci* 38:4777–4782
- Martin RB, Burr DB, Sharkey NA (1998) *Skeletal tissue mechanics*. Springer, New York
- Meyers MA, Chen PY, Lin AYM, Seki Y (2008) Biological materials: Structure and mechanical properties. *Prog Mater Sci* 53:1–206. doi:10.1016/j.pmatsci.2007.05.002
- Nyman JS, Roy A, Shen XM, Acuna RL, Tyler JH, Wang XD (2006) The influence of water removal on the strength and toughness of cortical bone. *J Biomech* 39:931–938. doi:10.1016/j.jbiomech.2005.01.012
- Olszta MJ, Cheng XG, Jee SS, Kumar R, Kim YY, Kaufman MJ, Douglas EP, Gower LB (2007) Bone structure and formation: a new perspective. *Mater Sci Eng R Rep* 58:77–116. doi:10.1016/j.mser.2007.05.001

- Orgel JP, Wess TJ, Miller A (2000) The in situ conformation and axial location of the intermolecular cross-linked non-helical telopeptides of type I collagen. *Struct Fold Des* 8:137–142
- Orgel JPRO, Irving TC, Miller A, Wess TJ (2006) Microfibrillar structure of type I collagen in situ. *Proc Natl Acad Sci USA* 103:9001–9005. doi:[10.1073/pnas.0502718103](https://doi.org/10.1073/pnas.0502718103)
- Orgel JPRO, Miller A, Irving TC, Fischetti RF, Hammersley AP, Wess TJ (2001) The in situ supermolecular structure of type I collagen. *Structure* 9:1061–1069
- Oyen ML (2008) The materials science of bone: lessons from nature for biomimetic materials synthesis. *MRS Bull* 33:49–55
- Parry DAD, Craig AS (1984) Growth and development of collagen fibrils in connective tissue. In: Ruggeri A, Motta PM (eds) *Ultrastructure of the connective tissue matrix*. Martinus Nijhoff, Boston, pp 34–63
- Perumal S, Antipova O, Orgel JPRO (2008) Collagen fibril architecture, domain organization, and triple-helical conformation govern its proteolysis. *Proc Natl Acad Sci USA* 105:2824–2829. doi:[10.1073/pnas.0710588105](https://doi.org/10.1073/pnas.0710588105)
- Posner AS (1969) Crystal chemistry of bone mineral. *Physiol Rev* 49:760–792
- Puxkandl R, Zizak I, Paris O, Keckes J, Tesch W, Bernstorff S, Purslow P, Fratzl P (2002) Viscoelastic properties of collagen: synchrotron radiation investigations and structural model. *Philos Trans R Soc B Biol Sci* 357:191–197. doi:[10.1098/rstb.2001.1033](https://doi.org/10.1098/rstb.2001.1033)
- Reid SA (1987) Micromorphological characterization of normal human-bone surfaces as a function of age. *Scanning Microsc* 1:579–597
- Rho JY, Kuhn-Spearing L, Zioupos P (1998) Mechanical properties and the hierarchical structure of bone. *Med Eng Phys* 20:92–102
- Rubin MA, Jasiuk I, Taylor J, Rubin J, Ganey T, Apkarian RP (2003) TEM analysis of the nanostructure of normal and osteoporotic human trabecular bone. *Bone* 33:270–282. doi:[10.1016/S8756-3282\(03\)00194-7](https://doi.org/10.1016/S8756-3282(03)00194-7)
- Sasaki N, Enyo A (1995) Viscoelastic properties of bone as a function of water-content. *J Biomech* 28:809–815
- Shen H, Li H, Brinson LC (2008) Effect of microstructural configurations on the mechanical responses of porous titanium: a numerical design of experiment analysis for orthopedic applications. *Mech Mater* 40:708–720. doi:[10.1016/j.mechmat.008.03.009](https://doi.org/10.1016/j.mechmat.008.03.009)
- Smith JW, Walmsley M (1959) Factors affecting the elasticity of bone. *J Anat* 93:503–523
- Traub W, Arad T, Weiner S (1989) 3-dimensional ordered distribution of crystals in turkey tendon collagen-fibers. *Proc Natl Acad Sci USA* 86:9822–9826
- Vincent JFV (1990) *Structural biomaterials*, revised edn. Princeton University, Princeton
- Wang XD, Puram S (2004) The toughness of cortical bone and its relationship with age. *Ann Biomed Eng* 32:123–135
- Weiner S, Wagner HD (1998) The material bone: structure mechanical function relations. *Ann Rev Mater Res* 28:271–298
- Yamashita J, Furman BR, Rawls HR, Wang XD, Agrawal CM (2001) The use of dynamic mechanical analysis to assess the viscoelastic properties of human cortical bone. *J Biomed Mater Res* 58:47–53